

Evolution of the hardness and Young's moduli of interlayers in Sn99Cu1/Cu solder joints subjected to isothermal ageing

Zhiwen Chen² · Changqing Liu² · Bing An³ · Yiping Wu³ · Li Liu^{1,4}

Received: 19 February 2017 / Accepted: 9 August 2017 / Published online: 21 August 2017
© Springer Science+Business Media, LLC 2017

Abstract The interlayers at solder/pad interface are critical to the reliability of solder joints; hence, their mechanical properties is of vital importance. However, the correlation between service duration and evolution of mechanical characteristics of these interlayers has seldom been reported. In this work, hardness and Young's moduli of Cu₆Sn₅, Cu₃Sn and Cu were evaluated by nanoindentation after ageing for every 100 h up to 500 h. It was found that hardness and Young's moduli of Cu₆Sn₅ and Cu₃Sn dropped with aging and reached the bottom at 200 h and 300 h, respectively, followed by a gradual increase. This U-shape curve was generally opposite to the evolution of corresponding parameters in Cu. Evolution of mechanical properties of IMCs can be attributed to constrained volume shrinkage induced by solid-state reactions that producing IMCs. The resultant stress ultimately affected load–displacement curves recorded by nanoindentation tests. The observed reverse evolution trend of examined parameters of Cu and adjacent IMC layers was a result of mutual constraint posed by Cu₃Sn/Cu interface.

1 Introduction

During reflow, intermetallic compounds (IMCs) that form at interfaces between solder alloys and their bonding pads provide mechanical and electrical interconnects in electronic packages. However, excessive growth of IMCs during reflow and subsequent ageing deteriorate the integrity of solder joints and hence reliability of electronic packages [1, 2]. In particular, for Sn-based solder joints, fractures in thick interfacial IMC layer are the primary failure mode in drop tests [3, 4]. Because of the close relationship between mechanical properties of IMCs and the reliability of electronic devices, characterizing mechanical properties of IMCs in macromechanical and nanomechanical regimes is of vital importance.

The thickness of IMC layer at solder/pad interface is normally at microscale, which poses substantial challenges in characterizing mechanical properties of IMC layers. Among various test technologies, nanoindentation is one of the most viable ways to evaluate mechanical properties of microstructures at microscale [5]. Generally, higher hardness indicates higher mechanical strength [6]. Therefore, some studies have been performed on thick IMC layers (approximately 20 μm) after long reflow or ageing times using nanoindentation to derive their Young's moduli and hardness [7]. Effects of strain rate and gain orientations on indentation results have also been reported [8, 9]. However, limited works were focused on potential effects of prolonged service durations on the evolution of mechanical properties of Cu–Sn IMC layers at solder/pad interface.

In this paper, a Sn99Cu1/Cu solder joint was aged at 175 °C from 0 to 500 h. The evolution of microhardness and Young's moduli of interlayers at Sn99Cu1/Cu interface, including Cu₆Sn₅ layer, Cu₃Sn layer and Cu substrate, was investigated by nanoindentation after ageing for different durations.

✉ Li Liu
l.liu@whut.edu.cn

¹ School of Materials Science and Engineering, Wuhan University of Technology, 122 Luoshi Road, Wuhan, Hubei, People's Republic of China

² Wolfson School of Mechanical, Electrical and Manufacturing Engineering, Loughborough University, Loughborough, Leicestershire LE11 3TU, UK

³ School of Materials Science and Engineering, Huazhong University of Science and Technology, 1037 Luoyu Road, Wuhan, Hubei, People's Republic of China

⁴ State Key Laboratory of Materials Processing and Die & Mould Technology, Huazhong University of Science and Technology, 1037 Luoyu Road, Wuhan 430074, Hubei, People's Republic of China

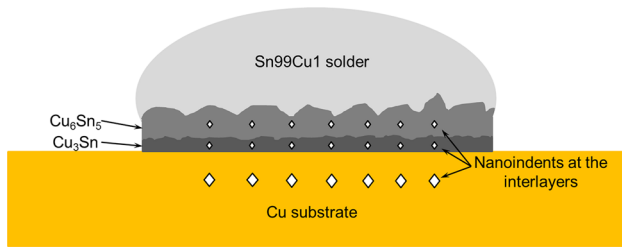


Fig. 1 Schematic of designated locations for nanoindents in solder joints

Table 1 Parameters and settings for nanoindentation tests

Specimen	Maximum depth (μm)	Termination	Loading rate (mN/s)	Unloading rate (mN/s)
Cu	1	Depth control	1	1
Cu_6Sn_5	0.3	Depth control	0.2	0.2
Cu_3Sn	0.3	Depth control	0.4	0.4

2 Experimental details

For sample preparation, Sn99Cu1 solder was reflowed on polycrystalline Cu sheet (purity: 99.9 wt%) at a peak temperature of 270 °C for 2 min. Specimens were then stored in a vacuum oven at 175 °C for 0–500 h. After every 100 h of ageing, specimens were removed, ground and polished using 0.05 μm colloidal silica to expose their interfacial microstructure and IMC layers. During sample preparation, no mounting was employed to avoid any potential effects caused by the contraction of resin. Nanoindentation tests were subsequently conducted on Cu_6Sn_5 layer, Cu_3Sn layer and Cu substrate (illustrated in Fig. 1) using a NanoTest Platform3 system. Seven indentation tests were carried out on each type of IMC with a horizontal interval of 20 μm . The drift rate of the test system was calibrated to be less than 0.05 nm/s prior to testing. A Vickers indenter was used at ambient temperature.

Parameters of nanoindentation tests at each layer are listed in Table 1. Initial loads, loading rates, maximum loads, unloading rates, dwelling periods and termination criteria for each test on different interlayers were set to be identical for comparison. Nominal strain rates for different interlayers was set between 0.03 and 0.04 s^{-1} , so that effect of strain rate on measured hardness was minimized [10]. Dwell periods at maximum load were set to zero to avoid effects of any possible creep on measured depth of indents [11]. Because of the micro-scale thickness of interfacial Cu_6Sn_5 and Cu_3Sn layers, depth of indents within interfacial IMC layers was set to 0.3 μm , so that nanoindents were within one specific IMC layer without interacting with adjacent material. Similarly, nanoindents in Cu were located approximately 10 μm from

$\text{Cu}_3\text{Sn}/\text{Cu}$ interface so that pile-up or sinking-in of Cu was accommodated within Cu portion during testing. Furthermore, in Sn99Cu1/Cu solder joint immediately after reflowing, Cu_6Sn_5 and Cu_3Sn layers are not visible under the microscope in NanoTest Platform3. Therefore, tests on Cu_6Sn_5 and Cu_3Sn layers started from solder joints aged at 175 °C for 100 h.

After nanoindentation tests, hardness of each interlayer after various ageing durations was derived from corresponding load–displacement curves using the software provided with NanoTest Platform3. The hardness of specimens, H , is defined as the average stress within contact area [12]:

$$H = F/A \quad (1)$$

where H is measured hardness, F is maximum force applied in nanoindentation test, and A is projected contact area of indents. Among the variables, F is directly recorded by the instrument, and A can be derived from the contact area–depth correlation of indenter.

In nanoindentation, reduced modulus (E_r) that accounts for the deformation of both specimen and indenter is defined as [13]:

$$E_r = \frac{1}{\beta} \frac{\sqrt{\pi}}{2} \frac{S}{\sqrt{A_c}} \quad (2)$$

where β is a constant with a value of 1.012 for Vickers indenter used in these tests; $S = \frac{dP}{dh}$, is contact stiffness which is defined as the slope of upper portion of unloading data; A_c is contact area, which can be derived from the shape function of Vickers indenter. Young's modulus of tested materials is related to reduced modulus by [14]:

$$\frac{1}{E_r} = \frac{1 - \nu^2}{E} + \frac{1 - \nu_i^2}{E_i} \quad (3)$$

where E and ν are Young's modulus and Poisson's ratio of tested materials, while E_i and ν_i are Young's modulus and Poisson's ratio of used indenter.

Because of the microscale depth of nanoindents in interlayers, possible effects of surface roughness on tests were also evaluated. After tests, indents in Cu, Cu_6Sn_5 and Cu_3Sn layers were profiled using a surface metrology instrument (Alicona Infinite Focus) with a vertical resolution of 10 nm. Therefore, influence of surface roughness of samples on indentation tests can be estimated.

3 Results

3.1 Nanoindentation

Figure 2 a, c and e show representative nanoindents within Cu and interfacial Cu_6Sn_5 and Cu_3Sn layers. It is shown

that nanoindents are located at the designated positions discussed in Sect. 2. Figure 2b, d and f show 3D models of typical indents in corresponding layers constructed from Alicona surface profiling results of nanoindents.

Because of the microscale size of nanoindents, potential influence of surface roughness of samples on nanoindentation tests was also evaluated on the basis of surface profiling results from Alicona system, with particular attention on the comparison between indentation depth and surface roughness. Profiles across the centre of nanoindents in Fig. 2 b, d, f are extracted and illustrated in Fig. 3. It shows that the average surface roughness of sample surface was approximately 20 nm. Compared with the depth of nanoindents (300–1000 nm), it is reasonable to conclude that effect of surface roughness on nanoindentation tests was minimal.

After nanoindentation tests, load–displacement curves were extracted. Average maximum load from the nanoindents in Cu_6Sn_5 layer is 7.4 mN, and those from indents in Cu_3Sn and Cu are 10.0 and 34.5 mN, respectively.

Example curves of nano indents from Cu_6Sn_5 , Cu_3Sn and Cu are illustrated in Fig. 4.

3.2 Evolution of hardness and Young’s modulus

After indentation testing, hardness of Cu_3Sn , Cu_6Sn_5 and Cu after ageing is evaluated using the analysis software in the instrument. Summary of hardness in different layers after prolonged aging are illustrated in Fig. 5. It is shown that hardness-duration curves for Cu_6Sn_5 and Cu_3Sn have a similar U shape. They reached their minimum values, 4.0 GPa and 4.5 GPa, at 200 and 300 h, respectively. And the average hardness are 5.9 ± 1.1 GPa for Cu_3Sn and 4.9 ± 1.8 GPa for Cu_6Sn_5 . In contrast, hardness of Cu was within a small range from 1.5 to 1.8 GPa, as illustrated in Fig. 5 c. It peaked after approximately 200 h of ageing, followed by a gradual decrease.

Table 2 lists average hardness of each layer after throughout aging. In general, these results show close agreement with reported values in literatures [7, 15]. It is worth of

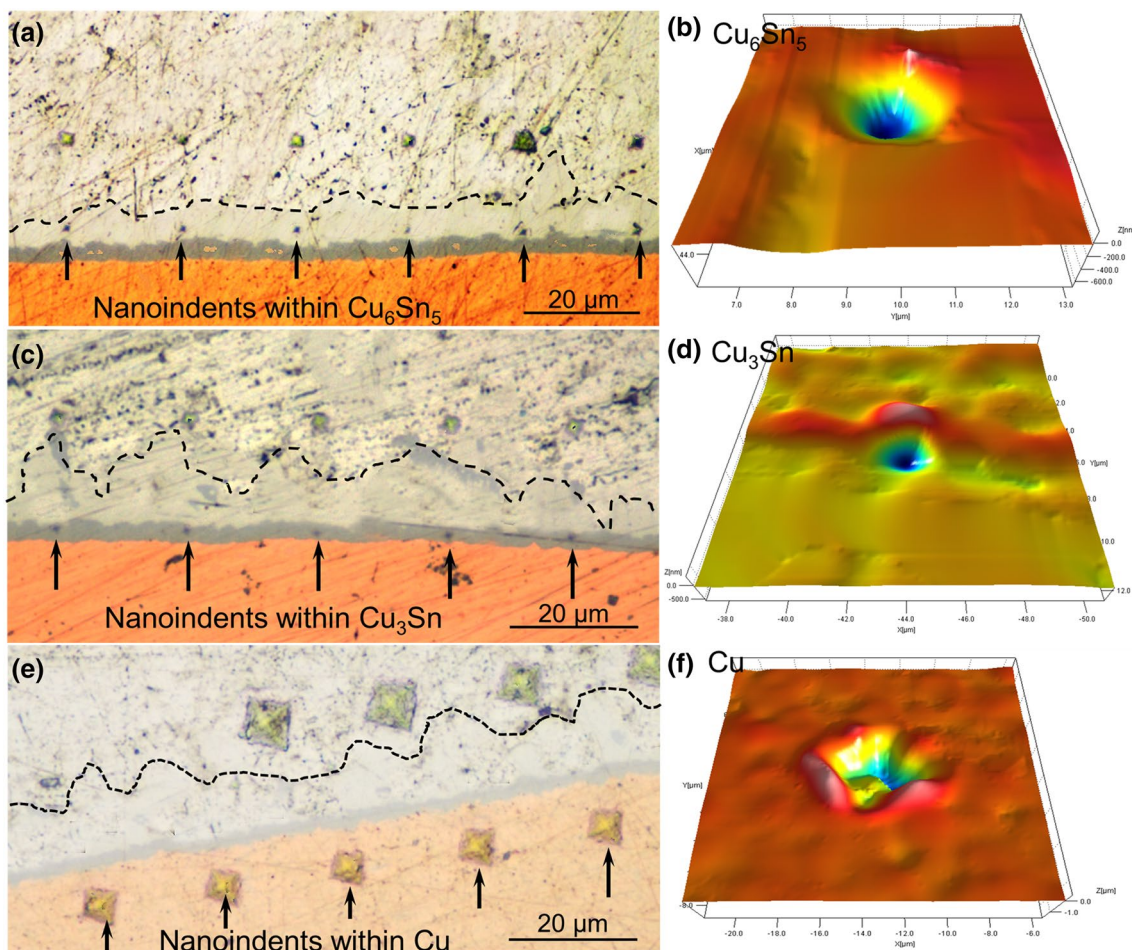


Fig. 2 Nanoindents in **a** Cu_6Sn_5 layer, **c** Cu_3Sn layer and **e** Cu substrate. Sub-figures **b**, **d**, **f** show the respective 3D profiles of indents in corresponding layers

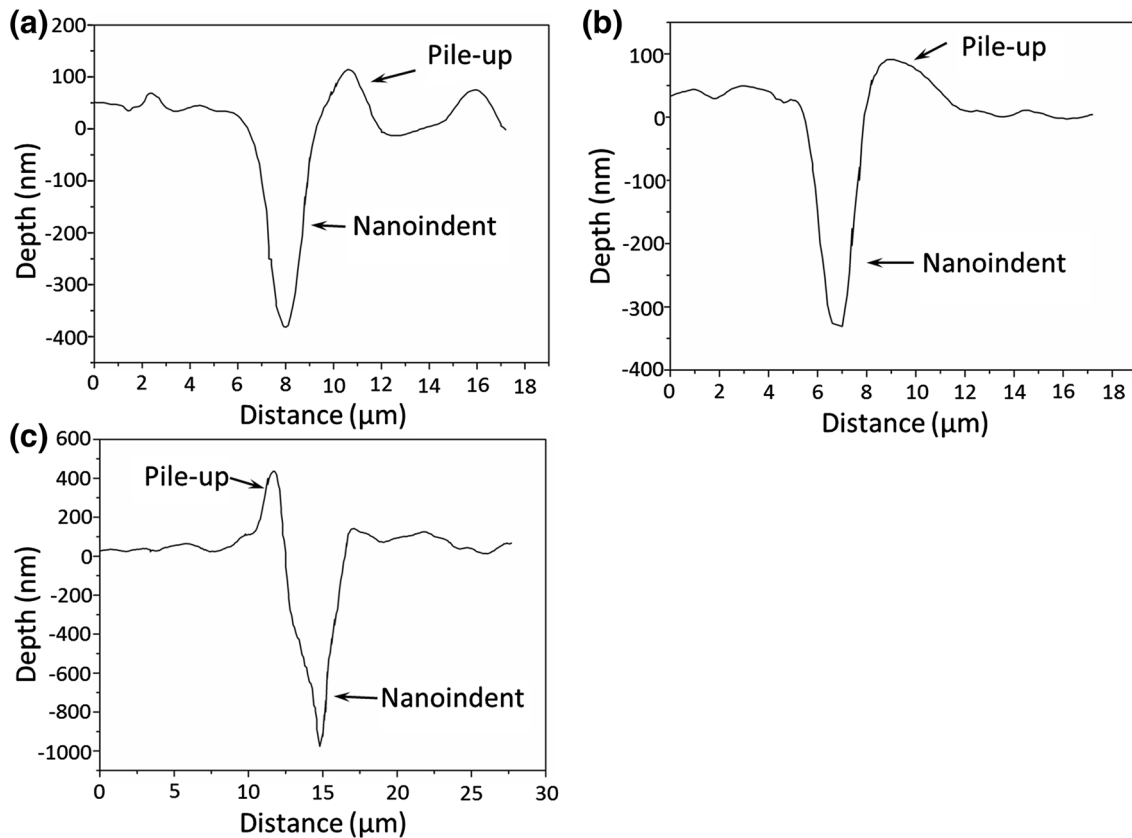


Fig. 3 Surface profiles across the centre of nanoindentations within **a** Cu_6Sn_5 layer, **b** Cu_3Sn layer and **c** Cu substrate

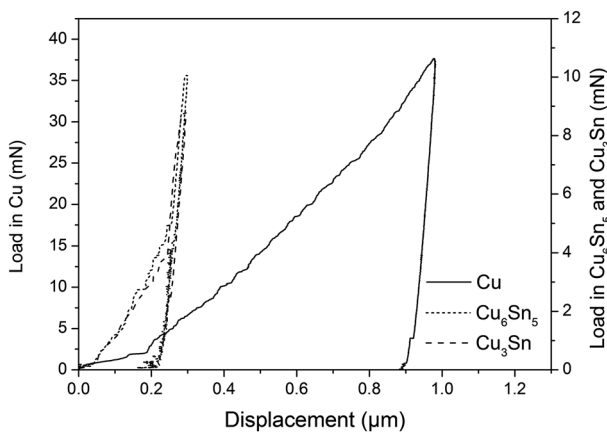


Fig. 4 Representative load–displacement curves from nanoindentations in Cu_6Sn_5 layer, Cu_3Sn layer and Cu substrate

notice that deviation in hardness of Cu_6Sn_5 is higher than that of Cu_3Sn , which is a result of different grain sizes of these two phases and influence of grain orientations. It has been reported that Cu_6Sn_5 grains are generally several times bigger than those of Cu_3Sn after ageing [9]. Therefore, nanoindentation on Cu_6Sn_5 is highly likely to be in

one single grain in each test, and different grain orientations of tested grains can pose significant effect on test results. For Cu_3Sn phase, several grains can be involved in one test, which can average out the influence from grain orientations.

Evolution of Young's moduli of Cu_3Sn , Cu_6Sn_5 and Cu after prolonged ageing is illustrated in Fig. 6. The Young's modulus–duration curve for Cu_6Sn_5 layer was generally in U-shape, with a valley of 60 GPa at 200 h. In the case of Cu_3Sn layer, a similar shape of curve can be identified and measured Young's modulus fluctuates between 134 and 155 GPa. By contrast, Young's modulus of Cu increased from 126 GPa at 100 h to 167 GPa at 200 h and remained relatively stable within the range of 142–158 GPa thereafter.

Average Young's moduli of Cu_6Sn_5 , Cu_3Sn and Cu after ageing are listed in Table 3. Experimental results from this work reasonably conforms with reported results [7, 15]. Higher variation in Young's modulus of Cu_6Sn_5 is resulting from the effect of grain orientations in different tests [9].

4 Discussion

In Figs. 5 and 6, it can be found that hardness and Young's moduli of Cu_6Sn_5 layer and Cu_3Sn layer evolved along a

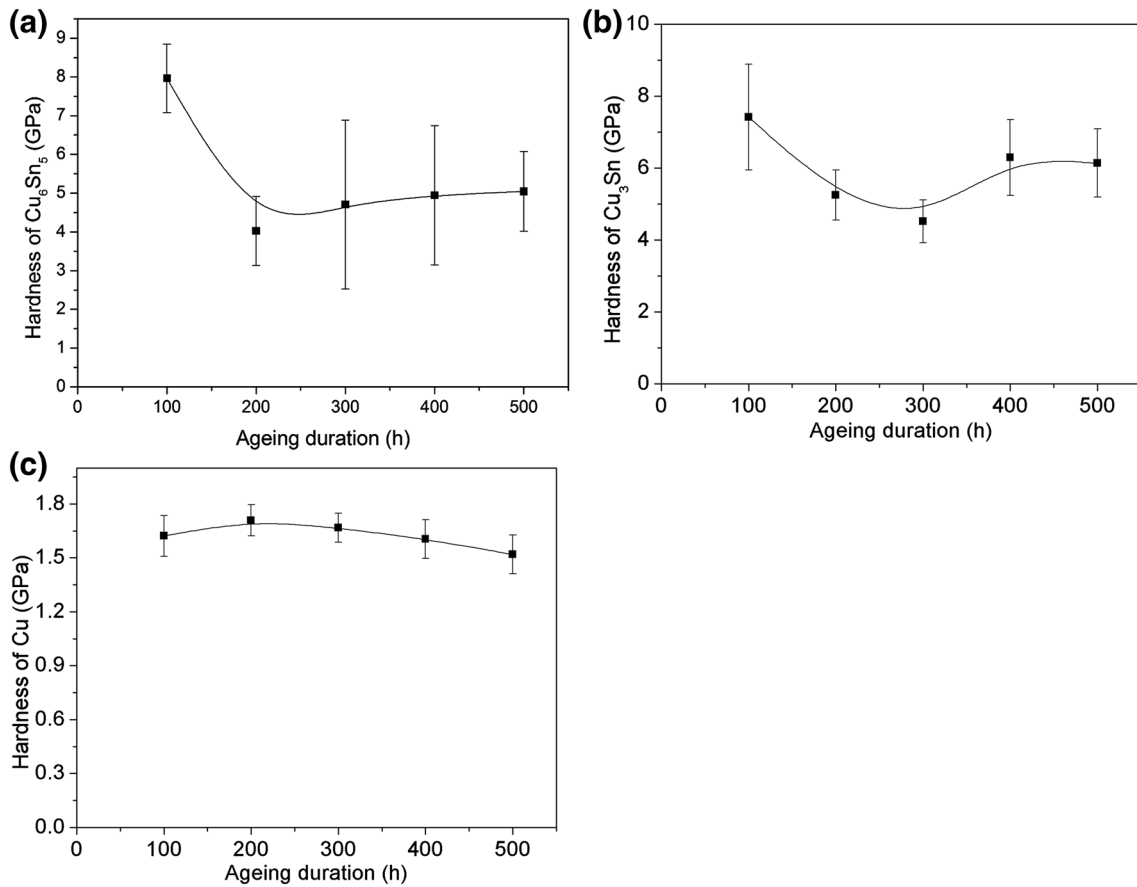


Fig. 5 Evolution of hardness within **a** Cu₆Sn₅ layer, **b** Cu₃Sn layer and **c** Cu substrate

Table 2 Comparison between the hardness obtained in this work and reported results

	Average hardness after ageing (GPa)	Reported hardness (GPa)
Cu ₆ Sn ₅	4.9 ± 1.8	6.1 ± 0.5 [7]
Cu ₃ Sn	5.9 ± 1.1	5.7 ± 0.6 [7]
Cu	1.6 ± 0.1	2.2 ± 0.2 [7]

similar trend, which is opposite to the trend for Cu. It has been reported that changes in hardness are closely related to stress state of a material [16, 17]. For a stressed specimen, the applied maximum load (F) should follow the relationship $F_{\text{compression}} > F_{\text{stress free}} > F_{\text{tension}}$ [18–21] at the same indentation depth, because the stress that acts as an additive load to resist penetration of an indenter into specimen varies with stress state within sample. Consequently, stress state can affect measured hardness of samples in nanoindentation tests. And a decrease in hardness indicates ascension of tensile stress within specimen.

From literatures, a volume shrinkage can be induced by solid-state reactions between Cu and Sn because of the

increase in densities after producing Cu₆Sn₅ and Cu₃Sn [22–25]. And this shrinkage is constrained by the attachment to adjacent substrate and solder, which ultimately results in development of stress within IMC layer [26]. So, it is highly likely that the observed evolution of hardness and Young’s modulus of Cu₆Sn₅ and Cu₃Sn is a result of volume shrinkage.

In nanoindentation, there is a constant ratio between hardness and tensile strength from Tabor’s model [27, 28],

$$H = 3\sigma_{\text{UTS}} \tag{4}$$

where σ_{UTS} is ultimate tensile strength (UTS), H is Vickers hardness.

In Fig. 5, the measured highest drop in hardness are 3.6 GPa for Cu₆Sn₅ (sample after aging for 100 and 200 h) and 2.2 GPa for Cu₃Sn (samples after aging for 100 and 300 h), respectively. Therefore, the induced change in UTS and corresponding tensile strain can be estimated as $\Delta \sigma_{\text{Cu}_6\text{Sn}_5} = -1.2$ GPa and $\Delta \epsilon_{\text{Cu}_6\text{Sn}_5} = -0.011$ for Cu₆Sn₅, and $\Delta \sigma_{\text{Cu}_3\text{Sn}} = 0.7$ GPa and $\Delta \epsilon_{\text{Cu}_3\text{Sn}} = -0.005$ for Cu₃Sn, where negative values indicate a drop in corresponding parameters. Given the fact that UTS and tensile fracture strain for a specific material is usually constant at room temperature, this drop in stress and strain is owing to different strain

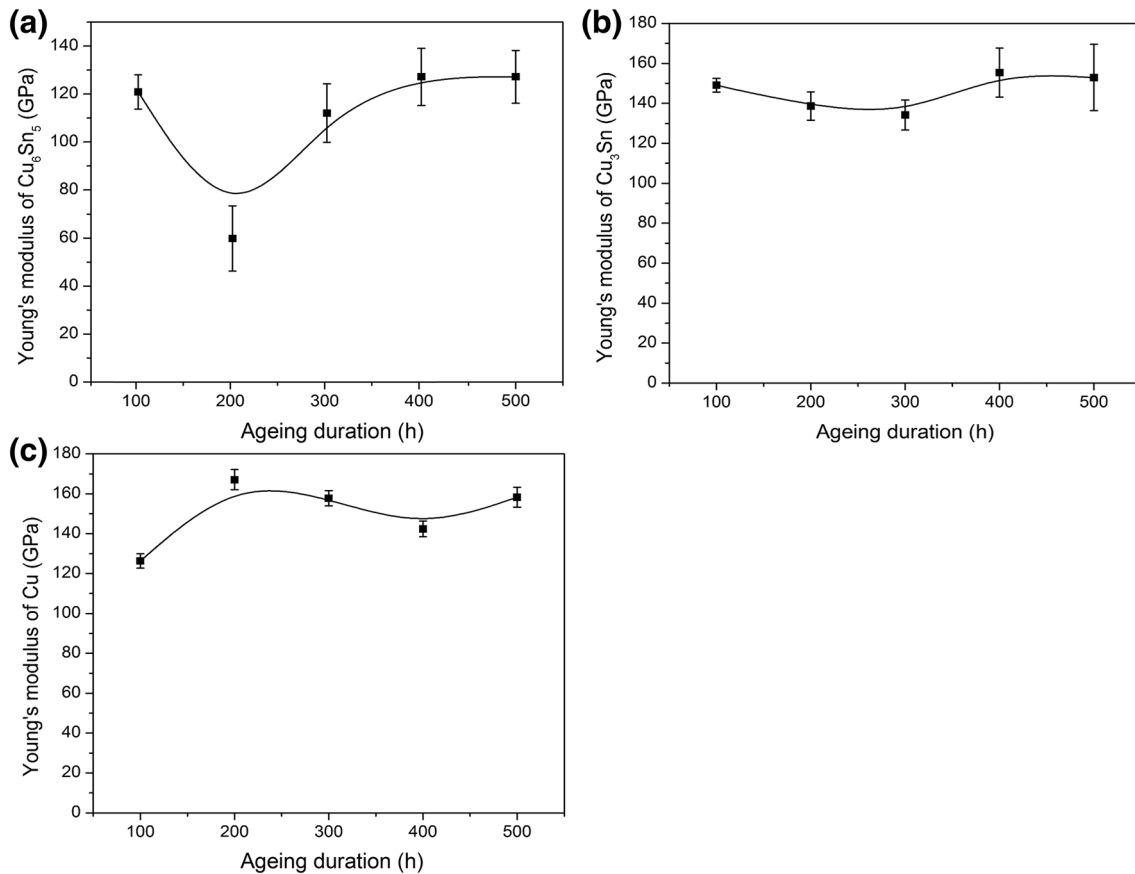


Fig. 6 Evolution of Young's moduli within **a** Cu_6Sn_5 layer, **b** Cu_3Sn layer and **c** Cu substrate

Table 3 Comparison between Young's moduli in this work and reported results

	Average E after ageing (GPa)	Reported E (GPa)
Cu_6Sn_5	109 ± 28	125 ± 7 [7]
Cu_3Sn	146 ± 9	136 ± 6 [7]
Cu	150 ± 16	111 ± 4 [7]

states (or start point of σ – ϵ curve) of the two samples in comparison. Therefore, it is reasonable to conclude that the experimental maximum tensile strain induced by volume shrinkage are $\epsilon_{\text{Cu}_6\text{Sn}_5} = 0.011$ and $\epsilon_{\text{Cu}_3\text{Sn}} = 0.005$.

Based on different densities of Cu, Sn, Cu_6Sn_5 and Cu_3Sn , theoretical tensile strains along one direction caused by volume shrinkage are 0.017 and 0.126 for Cu_6Sn_5 and Cu_3Sn , respectively [22]. It can be found that tensile strain by volume shrinkage for Cu_6Sn_5 in this work is close to theoretical value, while there is a notable difference between the two values for Cu_3Sn .

However, it should be noticed that numerical analysis on tensile strain by volume shrinkage is based on calculation without any account of the material. From literatures,

because of microstructural evolution, volume shrinkage induced by Cu–Sn interfacial reactions in aging does not necessarily fully convert to tension stress within IMCs. It has been reported that volume shrinkage can be relieved by formation of voids within IMCs in Ni–Sn and Cu–Sn system [29, 30]. Besides, formation of Kirkendall voids [31] close to $\text{Cu}_3\text{Sn}/\text{Cu}$ interface can also significantly attenuate the constraint and lower the stress level within Cu_3Sn because of resultant discontinuity in microstructure.

For Young's modulus, from Eq. 2 and Eq. 3, there is no direct correlation between stress and elastic modulus. However, a higher Young's modulus is a result of higher contact stiffness, which means the drop in load is more evident when indenter withdraws the same depth. This process is dominated by resistant stress from sample and increase of tension stress within IMC layer can surely lower it. Consequently, ascension in tension stress within tested sample can reduce measured Young's modulus in nanoindentation tests. Similar phenomenon has also been reported by other researchers in tests on other materials [32–34].

Therefore, both measured hardness and Young's modulus is related to the stress state within IMC layer, and these two parameters reached the bottom after the same aging duration

for both Cu_6Sn_5 and Cu_3Sn , as illustrated in Figs. 5 and 6. The followed slight increase can probably be a result of microstructural evolution. Build-up of stress can be partly relieved by formation of voids. And, interstitial diffusion of Cu in Sn and the diffusion in reverse direction can turn the initial tension stress to compressive stress during isothermal aging [26]. Therefore, with longer aging, tension stress within IMC layers fell gradually, and measured hardness and Young's modulus slightly ascended.

For hardness and Young's modulus of Cu, both parameters evolved in reverse trend in comparison to those of Cu_3Sn . This is probably due to the mutual constraint between Cu_3Sn and Cu. And microstructural recovery of Cu can also contribute to the fall of its hardness and Young's modulus after they peaked at 200 h.

Since failures of interconnections are frequently located within Cu_6Sn_5 and Cu_3Sn layers, this U-shape evolution of mechanical properties of interlayers implies that there is probably a sensitive aging duration for Sn-based solder/Cu solder joints. To be more specific, after aging for a certain period, Sn-based solder/Cu solder joints should be more prone to fail under tensile load because of the ascension of tensile stress resulted from volume shrinkage within IMC layer.

5 Conclusions

The hardness and Young's moduli of the interfacial Cu_6Sn_5 layer, Cu_3Sn layer and Cu substrate in Sn99Cu1/Cu solder joints were evaluated using nanoindentation tests after 0–500 h of ageing. Our conclusions based on the presented results and discussion are as follows:

1. Throughout the ageing at 175 °C, the average hardness of the interlayers was 4.6 ± 2.0 GPa for Cu_6Sn_5 , 5.9 ± 1.1 GPa for Cu_3Sn and 1.6 ± 0.1 GPa for Cu.
2. After the solder joints were aged for progressively increasing durations, the average Young's moduli of the different interlayers were 109 ± 28 GPa for Cu_6Sn_5 , 146 ± 9 GPa for Cu_3Sn and 150 ± 16 GPa for Cu.
3. The hardness and Young's moduli for Cu_6Sn_5 and Cu_3Sn layers evolved similarly. These parameters reached the lowest point after aging for 200 h for Cu_6Sn_5 and 300 h for Cu_3Sn , followed by a slight ascension. This U-shape evolution can be attributed to increase in tensile stress within IMC layer induced by volume shrinkage in solid-state reactions.
4. Throughout ageing, Young's modulus and hardness of Cu generally evolved in a reverse trend in comparison to those of Cu_3Sn , though fluctuations in hardness of Cu was within smaller range. The opposite evolution in mechanical properties of the two adjacent layers was a result of mutual constraint and volume shrinkage in IMC.

Acknowledgements This research was supported by a Marie Curie International Research Staff Exchange Scheme Project within the 7th European Community Framework Programme, No. PIRSES-GA-2010-269113, entitled "Micro-Multi-Material Manufacture to Enable Multifunctional Miniaturised Devices (M6)," the National Natural Science Foundation of China (No: 60976076), and a China-European Union technology cooperation project, No. 1110. The authors also acknowledge the open funding via State Key Laboratory of Materials Processing and Die & Mould Technology (No: P2018-018).

References

1. S. Ahat, M. Sheng, L. Luo, J. Electron. Mater. **30**, 10 (2001)
2. Y.C. Chan, A.C.K. So, J.K.L. Lai, Mater. Sci. Eng. B Adv. **55**, 1–2 (1998)
3. M. Date, T. Shoji, M. Fujiyoshi, K. Sato, K.N. Tu, Scripta Mater. **51**, 7 (2004)
4. J.Y. Kim, J. Yu, S.H. Kim, Acta Mater. **57**, 17 (2009)
5. I. Shohji, T. Nakamura, F. Mori, S. Fujiuchi, Mater. Trans. **43**, 8 (2002)
6. A.K. Gain, Y.C. Chan, W.K.C. Yung, Microelectron. Reliab. **51**, 5 (2011)
7. G.-Y. Jang, J.-W. Lee, J.-G. Duh, J. Electron. Mater. **33**, 10 (2004)
8. P.-F. Yang, Y.-S. Lai, S.-R. Jian, J. Chen, R.-S. Chen, Mater. Sci. Eng. A Struct. **485**, 1–2 (2008)
9. D. Mu, H. Huang, K. Nogita, Mater. Lett. **86**, (2012)
10. L. Shen, P. Lu, S. Wang, Z. Chen, J. Alloy Compd. **574**, (2013)
11. T. Chudoba, F. Richter, Surf. Coat. Technol. **148**, 2–3 (2001)
12. K.O. Kese, Z.C. Li, B. Bergman, J. Mater. Res. **19**, 10 (2004)
13. W. Wang, K. Lu, J. Mater. Res. **17**, 9 (2002)
14. W.C. Oliver, G.M. Pharr, J. Mater. Res. **7**, 6 (1992)
15. S. Lotfian, J.M. Molina-Aldareguia, K.E. Yazzie, J. Llorca, N. Chawla, J. Electron. Mater. **42**, 6 (2013)
16. S. Carlsson, P.L. Larsson, Acta Mater. **49**, 12 (2001)
17. J.G. Swadener, B. Taljat, G.M. Pharr, J. Mater. Res. **16**, 7 (2001)
18. Y.-H. Lee, D. Kwon, J. Mater. Res. **17**, 4 (2002)
19. T.Y. Tsui, W.C. Oliver, G.M. Pharr, J. Mater. Res. **11**, 3 (1996)
20. A. Bolshakov, W.C. Oliver, G.M. Pharr, J. Mater. Res. **11**, 3 (1996)
21. S. Suresh, A.E. Giannakopoulos, Acta Mater. **46**, 16 (1998)
22. Z. Chen, C. Liu, Y. Wu, B. An, L. Zhou, J. Electron Mater. **44**, 11 (2015)
23. P.L. Tu, Y.C. Chan, K.C. Hung, J.K.L. Lai, IEEE Trans. Adv. Pack. **23**, 4 (2000)
24. B.Y. Wu, H.W. Zhong, Y.C. Chan, M.O. Alam, J. Mater. Sci. **17**, 11 (2006)
25. C.-B. Lee, S.-B. Jung, Y.-E. Shin, C.-C. Shur, Mater. Trans. **43**, 8 (2002)
26. J.Y. Song, J. Yu, T.Y. Lee, Scripta Mater. **51**, 2 (2004)
27. P. Zhang, S.X. Li, Z.F. Zhang, Mater. Sci. Eng. A Struct. **529**, 62–73 (2011)
28. I.M. Hutchings, J. Mater. Res. **24**, 3 (2009)
29. C.C. Li, C.K. Chung, W.L. Shih, C.R. Kao, Metall. Mater. Trans. A **45**, 5 (2014)
30. S.J. Wang, L.H. Hsu, N.K. Wang, C.E. Ho, J. Electron. Mater. **43**, 1 (2014)
31. D. Kim, J.-H. Chang, J. Park, J.J. Pak, J. Mater. Sci. **22**, 7 (2011)
32. K. Yamaguchi, H. Adachi, N. Takakura, Met. Mater. **4**, 3 (1998)
33. S.L. Bazhenov, A.K. Rogozinskii, S.S. Evstiforov, A.A. Berlin, Dolk. Phys. Chem. **3433**, 2 (2010)
34. J.A. Benito, J. Jorba, J.M. Manero, A. Roca, Metall. Mater. Trans. A, **36**, 3317 (2005)